LIMNOLOGY
and
OCEANOGRAPHY: METHODS

ASLO

Limnol. Oceanogr.: Methods 2026, e70030

doi: 10.1002/lom3.70030

NEW METHODS

Chemical stabilization of glass microfiber type F filters for measuring particulate phosphorus using the extra high-temperature dry combustion method

Ying-Yu Hu [1]*, **Andrew J. Irwin** [2], **Zoe V. Finkel** [1]

[1]Department of Oceanography, Dalhousie University, Halifax, Canada; [2]Department of Mathematics and Statistics, Dalhousie University, Halifax, Canada

Abstract

Accurate quantification of particulate phosphorus is critical for understanding biogeochemical processes in aquatic systems. Extra high-temperature dry combustion at 800°C improves phosphorus recovery by ~11% compared to lower-temperature methods. Glass microfiber type F (GF/F) filters are often used for particulate carbon, nitrogen, and phosphorus analysis but melt at 800°C, entrapping phosphorus within the melted matrix and leading to poor phosphorus recovery, thereby limiting their compatibility with the extra high-temperature dry combustion method. To address this limitation, we show that adding 3200 μmol of magnesium sulfate ($MgSO_4$) yields statistically equivalent recoveries of total particulate phosphate from both laboratory-grown phytoplankton and seawater particulate matters collected on 25 mm GF/F filters, comparable to recoveries from 25 or 47 mm polycarbonate filters. We hypothesize that $MgSO_4$ reacts with SiO_2 in the GF/F filter matrix to form crystalline $MgSiO_3$, increasing the thermal stability of the filters (melting point >1000°C). This transformation preserves filter structure during the 800°C combustion and enables complete recovery of KH_2PO_4 and particulate phosphorus. Structural and chemical changes to the GF/F filter due to $MgSO_4$ addition were confirmed by scanning electron microscopy, energy-dispersive X-ray spectroscopy, and X-ray diffraction. The addition of $MgSO_4$ to GF/F increases their thermal stability, making them suitable for the extra high-temperature dry combustion method; consequently, particulate carbon, nitrogen and phosphorus samples can all be collected and analyzed on 25 mm GF/F filters, improving the consistency of particulate C : N : P estimates in aquatic biogeochemistry.

Accurately quantifying carbon (C), nitrogen (N), and phosphorus (P) is critical for understanding biogeochemical cycling and nutrient dynamics in aquatic ecosystems. Among these elements, P plays a central role in regulating primary production, trophic interactions, and ecosystem stability (Kwiatkowski et al. 2018; Lomas et al. 2022). Various methods are commonly used to measure particulate phosphorus in aquatic systems. Dry combustion at 450–500°C has been widely used to release P for analysis, including 550°C (Saunders and Williams 1955; Lomas et al. 2010), 450–500°C (Solórzano and Sharp 1980), and 450°C (Karl et al. 1991). Our recent study (Hu et al. 2022) showed this temperature range does not completely decompose all organic P compounds, underestimating total particulate P. We therefore developed the extra-high temperature dry combustion (X-HTDC) ash/hydrolysis method, which uses a combustion temperature of 800°C for a more complete decomposition of organic P compounds. This method improves total particulate P recovery by an average of 11% across phytoplankton cultures and particulate material collected from natural seawater samples compared to the lower-temperature combustion methods. The most significant

*Correspondence: ruby.hu@dal.ca

Associate editor: Robert Chen

improvements are seen in samples rich in phospholipids, polyphosphate, and nucleic acids—particularly from taxa such as cyanobacteria (e.g., *Crocosphaera*, *Synechococcus*), chlorophytes (e.g., *Chloroparvula pacifica*), and diatoms (e.g., *Minutocellus polymorphus*, *Thalassiosira pseudonana*). By improving the accuracy of P quantification, the X-HTDC method enhances our ability to detect shifts in elemental C : N : P and provides a stronger foundation for interpreting processes that impact carbon sequestration, ocean acidification, and phosphorus biogeochemistry.

Researchers commonly use pre-combusted 25 mm glass microfiber type F (GF/F) filters for particulate carbon and nitrogen analyses and often collect particulate phosphorus on a separate pre-combusted 25 mm GF/F filter to maintain consistent filtration conditions and biomass capture. Although GF/F filters have a nominal pore size of 0.7 μm, pre-combustion reduces their effective pore size to ~ 0.3 μm (Nayar and Chou 2003). Our X-HTDC method provides complete P recovery when using polycarbonate (PC) filters, which fully decompose at 800°C without leaving interfering residues. However, PC filters are unsuitable for C and N analysis due to their high carbon background, which interferes with C and N quantification. In contrast, we show GF/F filters melt at 800°C, entrapping P within the collapsed silica matrix of the filter, resulting in poor P recovery. Using PC filters for P and GF/F filters for C and N analyses can introduce biases in C and N vs. P biomass collection, compromising estimates of C : N : P, due to differences in pore size, particle retention, and the physical and chemical matrix of the different filter types particularly in communities with a range of cell sizes. To solve this issue, we have developed a method to alter the thermal characteristics of the 25 mm GF/F filters and make them suitable for use in the X-HTDC method. Specifically, we tested whether chemical stabilization with $MgSO_4$ could prevent GF/F matrix from melting and facilitate reliable P recovery at 800°C. Our approach is currently limited to 25 mm GF/F filters; we do not extend this method to other glass microfiber filter sizes or types, which may differ in mass or silica composition and require additional optimization.

$MgSO_4$ is the most commonly used ashing auxiliary in dry combustion methods for phosphorus analysis (Solórzano and Sharp 1980). In the current X-HTDC method, 34 μmol of $MgSO_4$ is added to each sample collected on a PC filter. Then $MgSO_4$ is dried and combusted with particulate phosphorus samples to minimize P volatilization during high-temperature combustion. It also promotes organic matter decomposition and increases the efficiency of subsequent acid hydrolysis (Hu et al. 2022). We have observed that diatom-rich samples dried with $MgSO_4$ consistently formed dark-red crystalline residues after X-HTDC. This coloration likely reflects the precipitation of biogenic silica by $MgSO_4$ (Rashid et al. 2011), and the subsequent formation of (Mg, Co)SiO_3, a compound with a high melting point of ~ 900°C. These observations led us to hypothesize that the addition of a sufficient amount of $MgSO_4$ might chemically convert the entire glass fiber matrix to $MgSiO_3$, thereby thermally stabilizing the filters at temperatures of 800°C and thus making them viable for use in the X-HTDC method.

Here we show that adding 3200 μmol $MgSO_4$ to each 25 mm GF/F filter effectively stabilizes the filter for combustion at 800°C, preventing melting and enabling complete recovery of KH_2PO_4 on GF/F filters. X-ray diffraction (XRD), scanning electron microscopy (SEM), and energy-dispersive X-ray spectroscopy (EDS) all confirm the conversion of amorphous SiO_2 in the GF/F filter to crystalline $MgSiO_3$ during combustion. To test particulate P recovery using the X-HTDC method with the stabilized GF/F filters, we compared recoveries from the marine diatom *Minutocellus polymorphus* (CCMP501) and Bedford Basin (NS, Canada) field samples collected on PC filters treated with 34 μmol $MgSO_4$ (applied to both 25 and 47 mm filters; Hu et al. 2022) and on 25 mm GF/F filters treated with 3200 μmol $MgSO_4$. Phosphorus recoveries were statistically indistinguishable between PC and the $MgSO_4$-stabilized GF/F filters, demonstrating that chemically modified GF/F filters are fully compatible with X-HTDC analysis. This modification stabilizes GF/F filters at 800°C and enables their use with the X-HTDC method, allowing consistent collection and analysis of C, N, and P on the same type of filter.

Materials and procedures

Reagents

All reagents were prepared in Milli-Q water (Millipore Direct 16). Potassium dihydrogen orthophosphate (KH_2PO_4, P-4550) was obtained from ACP Chemicals. Magnesium sulfate anhydrous ($MgSO_4$, M65500) was obtained from Fisher Scientific. Ammonium molybdate tetrahydrate (09878) and L-ascorbic acid (A5960) were obtained from Sigma-Aldrich. Other chemicals were analytical reagent grade.

Instruments

The muffle furnace (F30428C) and the microplate reader (Varioskan LUX with SkanIt Software for Microplate Readers RE, version 6.0.1.6) were from Thermo Scientific, the shaking incubator (LSE 6753) was from Corning, and the 96-well microplates (655101) were obtained from Greiner. Microcentrifuge tubes used for the colorimetric reaction were made of polypropylene. Porcelain crucibles (Fisherbrand™ J120) and crucible covers (Fisherbrand™ J128) were from Fisher Scientific.

Cleaning procedures

All glassware was cleaned with phosphate-free detergent, then with 5% v/v HCl and thoroughly rinsed with reverse osmosis water.

The 25-mm GF/F filters were incubated in 0.2 M HCl at 90°C for 30 min, thoroughly rinsed with reverse osmosis water until the rinse water tested neutral (pH ~ 7 using pH strips), then dried prior to pre-combustion at 450°C for 4 h.

Porcelain crucibles were cleaned with phosphate-free detergent and then rinsed with reverse osmosis water. Crucibles were filled with 0.2 M HCl (about 80% full), covered with lids, and heated at 90°C for 30 min. After the acid was removed, crucibles were rinsed with reverse osmosis water, given a final rinse with Milli-Q water, covered and dried completely in a gravity oven. Crucibles were heated up to 500°C at a ramp-rate of 150°C h^{-1} and then combusted at 500°C for 6 h. Crucibles were numbered with oil-based white sharpie (Sharpie, SKU35558) on the crucible lids.

X-ray diffraction analysis

After combustion, the GF/F filters were gently ground into a fine powder using an agate mortar and pestle. The powdered samples were then mounted onto microscope slides with double-sided tape for XRD analysis. A Siemens D-5000 powder diffractometer operating in Bragg–Brentano geometry was used. The diffractometer was equipped with a Cu target X-ray tube and a diffracted beam monochromator. The powdered samples were scanned between $2\theta = 15$–$80°$ with a step size of 0.04° and a counting time of 10 s per step to identify the crystalline phases present in the combustion residues.

XRD data were analyzed using Match! software (Crystal Impact) with the PDF–4+ database; phase identification was performed using the Crystallography Open Database. Peaks were matched to reference entries for $MgSiO_3$ (PDF 96-231-0967 and PDF 96-154-8550) and SiO_2 (PDF 96-153-6407, PDF 96-900-2650, and PDF 96-153-5067). Minor shifts in best-fit PDF selection likely reflect differences in signal quality, peak overlap, and relative peak intensities rather than distinct reaction pathways.

The software reported the estimated molar percentages of crystalline phases, including SiO_2, $MgSiO_3$ and others, based on reference pattern matching. Molar percentages of SiO_2 and $MgSiO_3$ are presented in Table 1 as reported by the software, without further normalization or residual estimation. Because Match! does not calculate formal error estimates for phase percentages, we have not included standard errors. However, relative abundances are semi-quantitative and primarily used for compositional comparison and the estimation of conversion from SiO_2 to $MgSiO_3$ using Eq. 1:

$$\%\text{Conversion} = 100 \times \frac{\text{molar}\,\%\,MgSiO_3}{\text{molar}\,\%\,MgSiO_3 + \text{molar}\,\%\,SiO_2} \quad (1)$$

Scanning electron microscopy and energy dispersive X-ray spectroscopy

The surface morphology and elemental composition of the samples were analyzed using a ThermoScientific Axia ChemiSEM equipped with a 70 mm^2 Silicon Drift Detector (SDD) for EDS. Samples were mounted on aluminum stubs using carbon tape and coated with a 15–20 nm layer of gold–palladium (Au–Pd) to enhance conductivity. Imaging was performed under high vacuum at an accelerating voltage of 5 kV, with a working distance ranging from approximately 5.6 to 8.9 mm, depending on magnification and detector requirements. EDS spectra were acquired with acquisition times ranging from 15 to 60 s per region, with average count rates between 9000 and 25,000 counts per second (cps), resulting in more than 250,000 total counts per spectrum.

Elemental analysis was conducted in both spot and mapping modes to determine elemental distribution across the combusted GF/F filters. Spot mode targeted specific microstructures and was used to quantify local elemental composition, while mapping mode scanned a broader area of the surface, producing a spatial distribution map of detected elements. Elemental quantification of both modes was performed using the instrument's integrated EDS software, which calculated molar concentrations of detected elements (C, O, Mg, Si, etc.) based on standardless peak deconvolution. For each selected region or spot, the molar Mg : Si ratio was calculated to assess the extent of chemical transformation from SiO_2 to $MgSiO_3$. Regions where Si was detected in the absence of Mg were interpreted as residual SiO_2, while regions showing co-presence of Mg and Si in an approximately 1 : 1 molar ratio were interpreted as $MgSiO_3$. To account for spatial heterogeneity, multiple spots were analyzed across the filter surface. Mean Mg : Si molar ratios and associated standard deviations were calculated separately for each class of regions (Si-only and Mg-Si) and are reported in Table 1.

Microalgal and seawater sample collection

The marine diatom *Minutocellus polymorphus* CCMP501 was obtained from the National Center for Marine Algae and Microbiota (NCMA). Cultures were grown in f/2 medium as described by Guillard and Ryther (1962). Cultures were maintained at an irradiance of 60 μmol m^{-2} s^{-1} on a 12 : 12 light–dark cycle and temperature of 20°C. At mid-exponential growth, 45 mL of culture was gently filtered onto 25 mm acid-washed and pre-combusted GF/F filters (Whatman, Cat # 1825-025) or 25 mm 0.4 μm PC filters (Isopore™, HTTP02500) using a vacuum pressure of less than 130 mmHg. Replicates were collected from four independent culture bottles to quantify variability. Blanks were PC filters or 25 mm acid-washed and pre-combusted GF/F filters with 45 mL of culture medium (without cells) filtered through.

Particulate matter from seawater was collected on 14th January 2025 from a depth of 10 m at 44.69°N, −62.36°W from the Bedford Basin (NS, Canada) using acid-cleaned sample bottles. In the lab, 1 L of seawater, prefiltered

through a 300 μm nylon mesh, was filtered onto a 25 mm acid-washed and pre-combusted GF/F filter and a 47 mm 0.2 μm PC filter (Nuclepore™, 10417012) under gentle vacuum pressure (< 130 mmHg). Note that 47 mm PC filters were used for collecting particulate phosphate from seawater samples (but not for the diatom culture samples) to accommodate the larger filtration volume (1 L vs. 45 mL) and to reduce the risk of clogging during vacuum filtration. Samples were collected in triplicate. To isolate cellular P, an oxalate reagent rinse was applied following Tovar-Sanchez et al. (2003), which removes any adsorbed P. To prepare blank samples, seawater was first filtered through a 0.2 μm, 142 mm PC filter (Isophore™, GTTP14250) using a Millipore® filter holder (YY3014236). Subsequently, 1 L of the filtered seawater was passed through the PC filters and 25 mm acid-washed and pre-combusted GF/F filters. For cellular P blanks, after filtering the pre-filtered seawater, the filters were also rinsed with oxalate.

All samples were flash-frozen in liquid nitrogen and then stored at −20°C until further processing.

Extra high-temperature dry combustion (X-HTDC)

Phosphate standard with GF/F filter

Phosphate standard solutions were prepared following Karl et al. (1991). About 1 g of KH_2PO_4 was transferred into an acid-washed glass beaker. The beaker was covered with foil and dried at 110°C for at least 2 h. KH_2PO_4 was cooled to room temperature in a vacuum desiccator. A primary standard of 1 mM was prepared by dissolving 0.1338 g dried KH_2PO_4 in 1 L Milli-Q water. The primary standard was stored in the fridge without adding chloroform.

In porcelain crucibles, 250 μL of the KH_2PO_4 primary standard was added to a single 25 mm GF/F filter (added P = 0.246 μmol). A $MgSO_4$ solution (2 M) was then added in volume of 200, 800, 1600, 1700, and 2400 μL, respectively, to obtain final amounts of 400, 1600, 3200, 3400, and 4800 μmol per filter. The procedural blank consisted of a crucible containing a single 25 mm GF/F filter and the corresponding volume of $MgSO_4$ solution for each treatment, but without KH_2PO_4.

Microalgal and seawater samples

Samples on 25 or 47 mm PC filters and pre-combusted 25 mm GF/F filters were dried with 34 and 3200 μmol $MgSO_4$ at 90°C, respectively. Procedural blanks were collected and processed in parallel and directly measured to correct for any background phosphorus.

X-HTDC procedure for all samples

The phosphate standard added to GF/F filters, and the microalgal and seawater particulate matter samples, were all combusted using the same extra high-temperature dry combustion (X-HTDC) procedure (Hu et al. 2022). The temperature was increased at a controlled rate of 150°C per hour until reaching 800°C, where it was maintained for 9 h. Crucibles were allowed to cool slowly to room temperature in the furnace.

Images of combusted filters (Fig. 1) were taken under ambient light using a cell phone camera (Samsung A52) positioned approximately 10 cm above the sample. The images were used to qualitatively assess filter morphology after combustion.

Hydrolysis and measurements of total particulate phosphorus

After the combusted samples and standards cooled, 5 mL of 0.2 M HCl was added directly to the ash in each crucible. Crucibles were then capped and incubated at 90°C for 30 min in an oven to hydrolyze acid-soluble phosphorus.

Colorimetric determination of phosphate followed the method of Chen et al. (1956). The molybdate reagent was a mixture of 2 parts Milli-Q water, 1 part 6 N sulfuric acid (1 mL 18 M H_2SO_4 and 5 mL Milli-Q), 1 part 2.5% ammonium molybdate (0.25 g ammonium molybdate topped to 10 g with Milli-Q in a 50 mL Falcon tube) and 1 part 10% ascorbic acid (1 g ascorbic acid topped to 10 g with Milli-Q in a 50 mL Falcon tube). Since ascorbic acid is sensitive to light, all solutions were prepared right before the measurement.

After mixing by pipetting up and down three times, about 2 mL of each hydrolysate was transferred to a 2 mL microcentrifuge tube and centrifuged at 13,000 rpm for 5 min at room temperature. Supernatants from samples and blanks, along with working standards (500 μL each), were then transferred into fresh 2 mL microcentrifuge tubes, and 500 μL molybdate reagent was added to each. Tubes were incubated at 37°C with continuous shaking at 200 rpm for 3 h for complete color development (Hu et al. 2022).

Duplicate 250 μL aliquots were transferred from each microtube to a microtiter plate. The plate was shaken for 5 s at 600 rpm, and absorbance was measured at 820 nm at room temperature. The apparent optical pathlength in the well was approximately 5 mm. Measured P was quantified from the analytical response using a calibration curve generated from eight standard working solutions ranging from 0 to 200 μM phosphate. The limit of detection was 6.13 nmol phosphate per sample.

KH_2PO_4 recovery was calculated using Eq. 2:

$$\%\text{Recovery} = 100 \times \frac{\text{Measured P}}{\text{Added P}} \quad (2)$$

Data analysis

Phosphorous content determined from phytoplankton culture and Bedford Basin seawater samples on GF/F and PC filters were compared using *t*-tests in R (version 4.4.2). One standard deviation is reported in the text, figures, and tables, unless otherwise noted.

Assessment

Morphological and structural transformations of GF/F filters under X-HTDC with varying $MgSO_4$ concentrations

The GF/F filter retained its original fibrous structure after combustion at 500°C (Fig. 1a). In contrast, combustion at 800°C led to distinct morphological changes depending on the amount of $MgSO_4$ added. When combusted with 34 μmol $MgSO_4$ (Fig. 1b)—a concentration used in our original X-HTDC method—the filters showed significant shrinkage and loss of structure due to melting at 800°C, followed by hardening upon cooling. Deformation was also observed in filters treated with 100 μmol (Fig. 1c) and 200 μmol (Fig. 1d) $MgSO_4$, while only minor structural changes were noticeable at 400 μmol $MgSO_4$ (Fig. 1e). At 800 μmol $MgSO_4$ (Fig. 1f), no visible melting or collapse was detected. At 3200 μmol $MgSO_4$ (Fig. 1g), the filter retained its overall shape but exhibited more pronounced morphological change compared to the fibrous texture seen in the unmodified filter when combusted at 500°C (Fig. 1a). This visible transformation reflects chemical restructuring, rather than melting or collapse. The original fibrous texture of glass fiber was replaced by a crystalline, sheet-like, brittle structure consistent with the formation of $MgSiO_3$, as confirmed by XRD analysis (Supporting Information Fig. S1; Table 1).

Scanning electron microscopy images revealed progressive structural changes in GF/F filters as $MgSO_4$ concentrations increased from 400 to 4800 μmol per filter (Fig. 2). As $MgSO_4$ additions increased, SEM images showed an increased abundance of well-defined, faceted structures consistent with crystalline morphology, forming denser deposits and larger aggregates on the GF/F filter surface. We refer to the fine-grained material coating the filter fibers as deposits, while we define the aggregates as larger, clustered particle masses that often obstruct pore spaces.

At 400 μmol, the filter showed well-defined microstructures, primarily composed of SiO_2 (cyan arrow) and $MgSiO_3$ crystals (orange arrow) identified in Fig. 2a. X-ray diffraction confirmed the formation of protoenstatite-phase $MgSiO_3$ (PDF 96-231-0967) with an orthorhombic crystal structure and lattice parameters $a = 9.25$ Å, $b = 8.74$ Å, and $c = 5.32$ Å (Smith 1959), consistent with hollow, elongated crystal clusters identified by EDS as having Mg : Si molar ratios near 1 : 1 (orange arrow; Fig. 2a). SiO_2 exhibited trigonal lattice (PDF 96-153-6407) parameters $a = 5.08$ Å and $b = 5.50$ Å (Di Ponponio and Continenza 1993), consistent with pea-shaped crystals identified by EDS as regions rich in silicon with no detectable magnesium (cyan arrow; Fig. 2a).

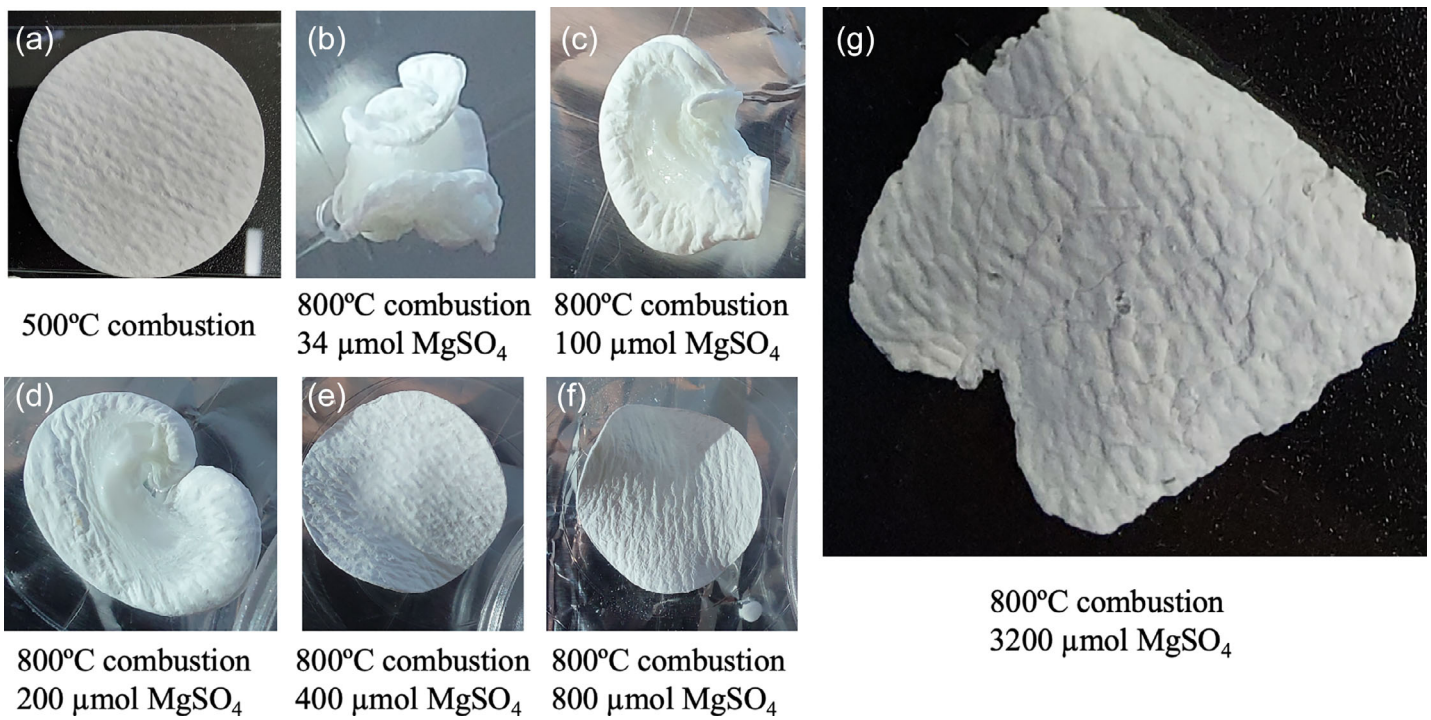

Fig. 1. After a 500°C combustion (**a**), the GF/F filter maintains its fibrous structure and does not melt. Filters combusted at 800°C with insufficient $MgSO_4$ (**b**: 34 μmol, **c**: 100 μmol and **d**: 200 μmol) exhibit visible melting and collapse. Partial shape retention is observed at 400–800 μmol $MgSO_4$ (**e** and **f**). At 3200 μmol $MgSO_4$ (**g**), the filter remains intact but appears visually altered. Images were captured using a cell phone camera and are presented for qualitative comparison only; no scale bar is included.

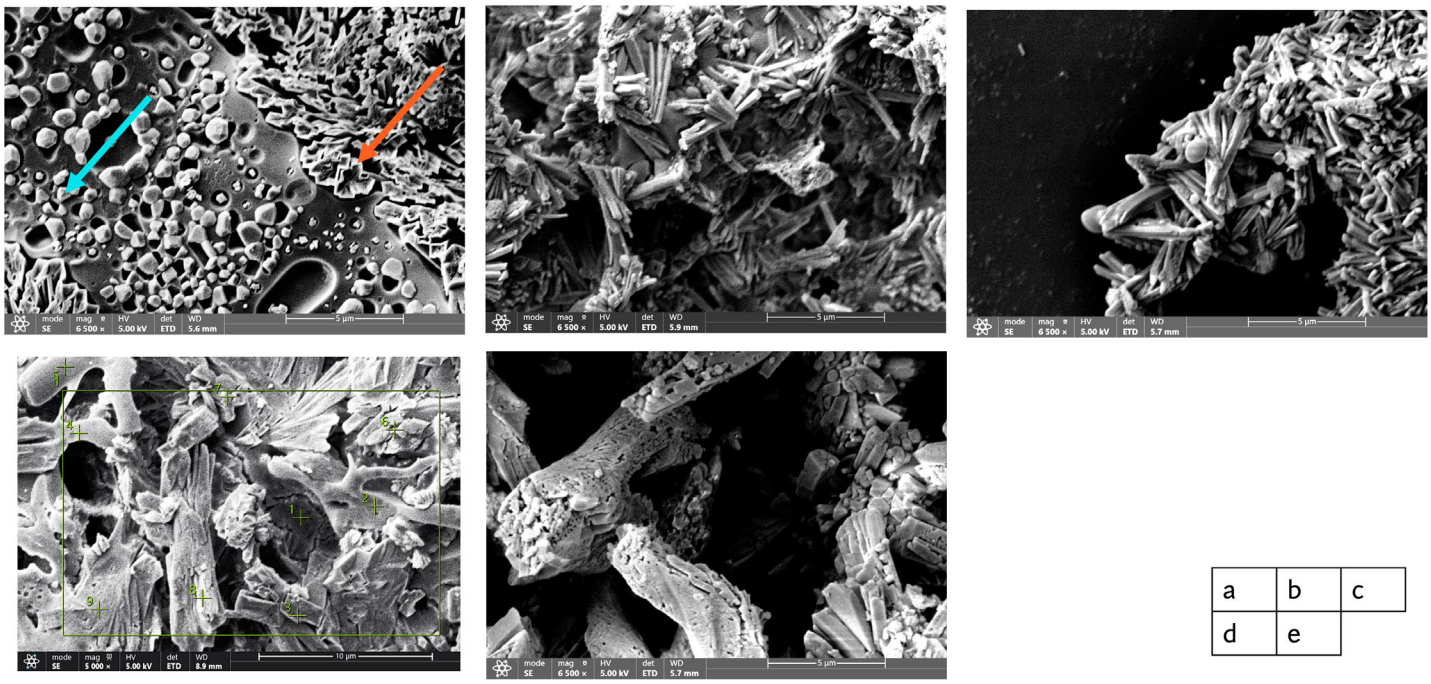

Fig. 2. Scanning electron microscopy (SEM) images of combusted 25 mm GF/F filters with varying amounts of $MgSO_4$ added: (**a**) 400 μmol, (**b**) 1600 μmol, (**c**) 3200 μmol, (**d**) 3400 μmol (note scale bar is 10 µm for this image only), and (**e**) 4800 μmol. In panel (**a**), representative SiO_2 and $MgSiO_3$ crystal morphologies are indicated by cyan and orange arrows, respectively. In panel (**d**), green crosses indicate EDS spot and mapping locations generated by the instrument software.

At 1600 and 3200 μmol $MgSO_4$ (Fig. 2b, c), EDS analysis detected no regions of the filter composed solely of Si, and Mg : Si molar ratios averaged ~ 1 : 1 (Table 1), indicating a shift toward $MgSiO_3$. Correspondingly, XRD quantified 4.3% and 0% molar SiO_2 at 1600 and 3200 μmol $MgSO_4$ treatments, respectively (Supporting Information Fig. S1b, c). At higher $MgSO_4$ levels (3400 and 4800 μmol, Fig. 2d, e), more extensive structural alternation was evident in SEM analysis, with dense, angular deposits distributed throughout the filter matrix. Although EDS continued to show no Si-only regions at 4800 μmol, XRD detected 3.0% molar SiO_2 (Supporting Information Fig. S1e), indicating the reappearance of residual SiO_2 at excessive $MgSO_4$ concentrations.

Table 1. Summary of KH_2PO_4 recovery and filter composition after X-HTDC combustion of 25 mm GF/F filters with varying $MgSO_4$ additions. Molar % SiO_2 and $MgSiO_3$ were identified based on XRD peak matches and analysis (Supporting Information Fig. S1). The SiO_2 : $MgSiO_3$ molar ratio was calculated from these molar percentages. KH_2PO_4 recovery from four replicates was calculated using Eq. 2 and reported as mean ± standard deviation. Elemental composition from EDS is reported as Mg : Si molar ratios for two phases: upper row (if present): SiO_2-rich phases (Mg : Si ≈ 0); and lower row: $MgSiO_3$-rich phases (Mg : Si ≈ 1), presented as mean ± standard deviation. The number of EDS measurement spots per sample (*n*) is indicated.

$MgSO_4$ added (μmol/filter)	SiO_2 (molar %)	$MgSiO_3$ (molar %)	SiO_2 : $MgSiO_3$ (molar ratio)	% KH_2PO_4 recovery mean ± SD ($n = 4$)	EDS Mg : Si	
					Mean ± SD	*n*
400	9.0	75.7	0.12	61.32 ± 3.52	0.05 ± 0.10	12
					0.90 ± 0.27	14
1600	4.3	75	0.06	75.78 ± 8.31	1.1 ± 0.35	6
3200	0	20.6	0	100.06 ± 0.48	0.84 ± 0.13	23
3400	10.8	71.3	0.15	91.21 ± 5.11	0.06 ± 0.03	3
					0.85 ± 0.08	6
4800	3.0	57.4	0.05	106.03 ± 7.29	0.82 ± 0.04	12

In summary, 800°C combustion with increasing $MgSO_4$ concentrations induced progressive morphological and mineralogical transformations in GF/F filters. XRD analysis indicated complete conversion of SiO_2 to $MgSiO_3$ at 3200 μmol $MgSO_4$; however, residual SiO_2 reappeared at higher concentrations. SEM imaging revealed denser, more angular mineral deposits distributed throughout the filter matrix at elevated $MgSO_4$ levels. These structural and compositional changes were accompanied by enhanced thermal stability: 25 mm glass microfiber filters treated with >800 μmol $MgSO_4$ retained their structure during combustion at 800°C, in contrast to the collapse or melting observed at lower $MgSO_4$ concentrations.

Optimizing $MgSO_4$ concentrations for KH_2PO_4 recovery at 800°C

Recovery of KH_2PO_4 was 61% with the addition of 400 μmol $MgSO_4$ per filter, likely due to phosphorus entrapment within the partially melted GF/F matrix during combustion at 800°C (Table 1). Each GF/F filter used in the study weighed approximately 35 mg, corresponding to $\sim$ 472 μmol SiO_2 (Cytiva 2023). Although no visible structural collapse was observed at 400 μmol $MgSO_4$ (Fig. 1e), the $MgSO_4$: SiO_2 molar ratio of 1 : 1 was insufficient for complete conversion of SiO_2 to $MgSiO_3$; XRD analysis still detected 9 mol% residual SiO_2. While high-temperature P volatilization is a known concern, our previous work (Hu et al. 2022) demonstrated that 34 μmol $MgSO_4$ is sufficient to prevent P volatilization at 800°C. Element P was not detected by SEM-EDS or XRD because the KH_2PO_4 dose applied (0.246 μmol per filter) was likely below the detection limit. We hypothesize that partially fused SiO_2 physically entrapped KH_2PO_4, shielding it from acid hydrolysis and contributing to low P recovery.

Between 400 and 3200 μmol $MgSO_4$ per filter, recovery of KH_2PO_4 increased steadily, coinciding with a marked decrease in residual SiO_2 and a corresponding increase in $MgSiO_3$ (Supporting Information Fig. S1; Table 1). At 400 μmol $MgSO_4$, $\sim$ 89% of the original SiO_2 in the 25 mm GF/F filter was already converted to $MgSiO_3$, but further $MgSO_4$ addition produced only small incremental increases in conversion ($\sim$ 1.8 μmol of SiO_2 per 100 μmol $MgSO_4$). Although the conversion plateaued at 88% (Eq. 1) in chemical and structural change, KH_2PO_4 recovery continued to improve, increasing by $\sim$ 1% per 100 μmol $MgSO_4$. With 3200 μmol $MgSO_4$, residual SiO_2 was no longer detected by XRD (Supporting Information Fig. S1; Table 1), indicating complete conversion of the filter matrix to $MgSiO_3$. Consistent with this transformation, KH_2PO_4 recovery also approached completion.

We did not test KH_2PO_4 recovery with $MgSO_4$ concentration below 400 μmol, as filter instability was already evident at these lower doses. Melting phenomena observed at or below 200 μmol $MgSO_4$ (Fig. 1b–d) further confirmed that insufficient $MgSO_4$ compromises filter stability under X-HTDC conditions.

Above 3200 μmol $MgSO_4$, residual SiO_2 reappeared in the XRD analysis, coinciding with reduced KH_2PO_4 recovery (91% at 3400 μmol $MgSO_4$). Recovery returned to near-complete at 4800 μmol $MgSO_4$, but with a larger variation ($\pm$ 7%). SEM images indicated that excess $MgSO_4$ led to denser mineral aggregates, which may have limited further SiO_2 conversion and entrapped phosphorus, thereby impeding subsequent acid hydrolysis and contributing to the reduced recovery or more variable recovery at higher $MgSO_4$ doses.

In summary, addition of 3200 μmol $MgSO_4$ to 25 mm GF/F filter effectively converted SiO_2 to $MgSiO_3$ and supported complete KH_2PO_4 recovery. However, excessive $MgSO_4$ additions led to the reappearance of SiO_2 and reduced phosphorus recovery, highlighting the importance of optimizing $MgSO_4$ dosage to balance filter thermal stability and P recovery under X-HTDC conditions.

Phosphorus from microalgal and seawater samples

To evaluate whether $MgSO_4$-stabilized GF/F filters could replace PC filters for P analysis using X-HTDC conditions, total particulate phosphorus (TPP) and cellular P (P_c) were measured from lab-cultured diatom and Bedford Basin seawater samples filtered onto PC filters and 25 mm GF/F filters. PC filters were treated with 34 μmol $MgSO_4$, consistent with previously published X-HTDC protocols, while GF/F filters were treated with 3200 μmol $MgSO_4$ as optimized in this study. There are no significant differences in TPP or P_c obtained by the two filter types for either sample source (Table 2).

Discussion

Our extra high-temperature dry combustion (X-HTDC) method that employs an 800°C combustion temperature improves P recovery by approximately 11% compared to lower-temperature methods that use 450–500°C for combustion (Hu et al. 2022). Although 25 mm GF/F filters are widely

Table 2. Total particulate phosphorus (TPP) and cellular phosphorus (P_c) from *Minutocellus polymorphus* CCMP501 (pmol cell^{-1}) and particulate matter from Bedford Basin seawater (μmol L^{-1}) collected on PC and GF/F filters. P content is reported as mean $\pm$ standard deviation. Sample sizes were $n = 4$ for CCMP501 and $n = 3$ for Bedford Basin samples. The *t*-test *p* value indicates no significant difference in P content between the two filter types ($p > 0.05$).

Sample source	Filter type	P content	*p*
CCMP501, TPP (pmol cell^{-1})	PC	0.011 $\pm$ 0.0006	0.480
	GF/F	0.011 $\pm$ 0.0013	
Bedford Basin, TPP (μmol L^{-1})	PC	0.068 $\pm$ 0.003	0.214
	GF/F	0.078 $\pm$ 0.010	
Bedford Basin, P_c (μmol L^{-1})	PC	0.055 $\pm$ 0.018	0.695
	GF/F	0.050 $\pm$ 0.004	

used for C and N analysis, they lack the thermal stability required for X-HTDC and tend to melt at elevated temperatures, causing poor P recovery (Table 1). To enable consistent biomass collection across C, N, and P analyses using the same filter type, we enhanced the thermal stability of GF/F filters by adding 3200 μmol of $MgSO_4$ to each 25 mm GF/F filter (containing $\sim$ 472 μmol SiO_2). We provide evidence that this treatment facilitates the conversion of SiO_2 to $MgSiO_3$, a compound capable of withstanding combustion temperatures above 1000°C (Singh et al. 2022), ensuring complete P recovery from particulate samples collected on 25 mm GF/F filters.

$MgSO_4$ decomposes over a broad temperature range (150–850°C), producing MgO, which reacts with SiO_2 to form $MgSiO_3$—a protoenstatite-phase crystal with an orthorhombic structure (François et al. 2016). The high-temperature resistance of $MgSiO_3$ (melting point > 1000°C) addresses the thermal instability of GF/F filters caused by the melting of SiO_2 under X-HTDC conditions, thereby preserving the integrity of structurally and chemically modified filters during combustion at 800°C. While reducing agents can promote $MgSO_4$ decomposition at lower temperatures, our study demonstrated partial decomposition of $MgSO_4$ at 800°C in air without a reducing agent. This aligns with prior reports showing significant decomposition of $MgSO_4$ between 800°C and 850°C (François et al. 2016), although complete decomposition typically requires temperature up to 900°C (Souza et al. 2020). Even when MgO is produced, the reaction between MgO and SiO_2 occurs only at points of physical contact, due to the solid-phase heterogeneity of the system. Thus, both thermal limitations and restricted surface interactions constrain $MgSiO_3$ formation. To overcome these constraints, a substantial excess of $MgSO_4$ is required. Our results show that complete SiO_2 to $MgSiO_3$ conversion was achieved for 25 mm GF/F filters only at 3200 μmol $MgSO_4$ per filter—well above the theoretical 1 : 1 molar ratio ($\sim$ 472 μmol SiO_2 per 25 mm GF/F filter).

The 61% recovery of KH_2PO_4 on GF/F filter at low $MgSO_4$ concentrations (400 μmol) and 800°C combustion is attributed to phosphorus entrapment within partially melted SiO_2 structures. Despite retention of gross filter morphology, SEM and XRD evidence indicate that this $MgSO_4$ dose was insufficient to fully convert SiO_2 in the 25 mm GF/F filter to $MgSiO_3$, resulting in the formation of fused silica regions that likely encapsulated KH_2PO_4 and hindered its release during acid hydrolysis. At $MgSO_4$ concentrations above 3200 μmol, there is a decline in phosphorus recovery to 91% associated with the reappearance of residual SiO_2 and the formation of dense, angular deposits across the filter matrix. SEM images at these higher concentrations suggest a tightly packed mineral structure that, while thermally stable, may have physically restricted (1) the contact between produced MgO and entrapped SiO_2—impeding complete conversion to $MgSiO_3$; and (2) the acid accessibility to entrapped phosphorus during hydrolysis. Although we did not directly measure density or acid permeability, these two regimes (1) melt-induced entrapment at low $MgSO_4$ and (2) matrix densification at high $MgSO_4$ share a similar outcome: reduced hydrolytic accessibility of phosphorus for subsequent measurement.

Together, these findings indicate that 3200 μmol $MgSO_4$ is the optimal concentration for 25 mm GF/F filter, balancing effective thermal stabilization of the filter with quantitative phosphorus recovery under X-HTDC conditions.

Comments and recommendations

The 25-mm glass microfiber type F (GF/F) filters have long been used to collect particulate carbon, nitrogen, and phosphorus for elemental analysis. However, their use for phosphorus measurement under our X-HTDC method was previously limited due to filter melting at extra high combustion temperatures (800°C), resulting in poor phosphorus recovery. In this study, we demonstrate that adding 3200 μmol $MgSO_4$ to each 25 mm GF/F filter converts the silica matrix to $MgSiO_3$, increasing its thermal stability from $\sim$ 500°C to above 1000°C. This chemical transformation during combustion preserves the filter's structure and prevents phosphorus from being entrapped in a collapsed matrix, thereby allowing complete P recovery. Particulate phosphorus recovered from GF/F filters chemically stabilized during combustion showed no significant difference from that recovered using PC filters combusted directly under the same X-HTDC conditions.

This chemical modification restores the compatibility of GF/F filters with our X-HTDC method, developed for a complete phosphorus recovery. It allows all three key particulate elements—C, N, and P—to be collected on the same filter type again, ensuring consistent biomass collection and enhancing the reliability of C : N : P stoichiometric estimates in aquatic biogeochemistry. Such consistency is especially valuable in field-based studies, where biological complexity already contributes substantial variability that can be further intensified by filter-specific differences in pore size and matrix texture. We anticipate that this advancement will facilitate broader adoption of X-HTDC approaches for phosphorus quantification and support more standardized elemental ratio measurements in aquatic ecosystem research.

Author Contributions

Ying-Yu Hu contributed to conceptualization, methodology, validation, formal analysis, investigation, resources, writing – original draft, and visualization. Andrew J. Irwin contributed to validation, resources, writing – review and editing, visualization, supervision, project administration, and funding acquisition. Zoe V. Finkel contributed to validation, resources, writing – review and editing, supervision, project administration, and funding acquisition.

Acknowledgments

This work was supported by the Simons Collaboration on Ocean Processes and Ecology/SCOPE-Gradients (Grant ID:

723789, Zoe V. Finkel) and the Simons Collaboration on Computational Biogeochemical Modeling of Marine Ecosystems/CBIOMES (Grant ID: 549937, Zoe V. Finkel). The authors thank Dr Nuwanthi Samarasinghe for contributing microalgae samples for the assessment, Elisa Dai and Pixie Owen for collecting Bedford Basin samples. The authors thank Andrew George (Physics and Atmospheric Science, Dalhousie University) for X-ray diffraction analysis and Dr Eric Moreau (Mechanical Engineering, Dalhousie University) for scanning electron microscopy analysis. The authors are especially grateful to the anonymous reviewers for their thoughtful comments and constructive suggestions, which significantly improved the clarity and quality of this manuscript.

Conflicts of Interest

None declared.

Data Availability Statement

X-ray diffraction, energy-dispersive X-ray spectroscopy, and scanning electron microscopy data that support the findings of this study are publicly available in Zenodo at https://doi.org/10.5281/zenodo.15792951.

References

Chen, P. S., T. Y. Toribara, and H. Warner. 1956. "Microdetermination of Phosphorus." *Analytical Chemistry* 28: 1756–1758. https://doi.org/10.1021/ac60119a033.

Cytiva. 2023. "Baseline Grade GF/F Datafile." https://cdn.cytivalifesciences.com/api/public/content/dB4t3NiLukGcEW7_8a9LEg-pdf.

Di Ponponio, A., and A. Continenza. 1993. "Structural Properties of α-Quartz Under High Pressure and Amorphization Effects." *Physical Review B* 48: 12558. https://doi.org/10.1103/PhysRevB.48.12558.

François, P., C. Szopa, A. Buch, et al. 2016. "Magnesium Sulfate as a Key Mineral for the Detection of Organic Molecules on Mars Using Pyrolysis." *Journal of Geophysical Research, Planets* 121: 61–74. https://doi.org/10.1002/2015je004884.

Guillard, R. R. L., and J. H. Ryther. 1962. "Studies of Marine Planktonic Diatoms: I. Cyclotella Nana Hustedt and Detonula Confervacea (Cleve) Gran." *Canadian Journal of Microbiology* 8: 229–239. https://doi.org/10.1139/m62-029.

Hu, Y.-Y., A. J. Irwin, and Z. V. Finkel. 2022. "Improving Quantification of Particulate Phosphorus." *Limnology and Oceanography: Methods* 20: 729–740. https://doi.org/10.1002/lom3.10517.

Karl, D. M., J. E. Dore, D. V. Hebel, and C. Winn. 1991. "Procedures for Particulate Carbon Nitrogen, Phosphorus and Total Mass Analyses Used in the US-JGOFS Hawaii Ocean Time-Series Program." In Marine Particles: Analysis and Characterization, 71–77. American Geophysical Union.

Kwiatkowski, L., O. Aumont, L. Bopp, and P. Ciais. 2018. "The Impact of Variable Phytoplankton Stoichiometry on Projections of Primary Production, Food Quality and Carbon Uptake in the Global Ocean." *Global Biogeochemical Cycles* 32: 516–528. https://doi.org/10.1002/2017GB005799.

Lomas, M. W., N. R. Bates, R. J. Johnson, D. K. Steinberg, and T. Tanioka. 2022. "Adaptive Carbon Export Response to Warming in the Sargosso Sea." *Nature Communications* 13: 1211. https://doi.org/10.1038/s41467-022-28842-3.

Lomas, M. W., A. L. Burke, D. A. Lomas, et al. 2010. "Sargasso Sea Phosphorus Biogeochemistry: An Important Role for Dissolved Organic Phosphorus (DOP)." *Biogeosciences* 7: 695–710. https://doi.org/10.5194/bg-7-695-2010.

Nayar, S., and L. M. Chou. 2003. "Relative Efficiencies of Different Filters in Retaining Phytoplankton for Pigment and Productivity Studies." *Estuarine, Coastal and Shelf Science* 58: 241–248. https://doi.org/10.1016/S0272-7714(03)00075-1.

Rashid, I., N. H. Daraghmeh, M. M. A. Omari, et al. 2011. "Magnesium Silicate." In Profiles of Drug Substances Excipients and Related Methodology, 241–285. Elsevier.

Saunders, W. M. H., and E. G. Williams. 1955. "Observation on the Determination of Total Organic Phosphorus in Soils." *Journal of Soil Science* 6: 254–267. https://doi.org/10.1111/j.1365-2389.1955.tb00849.x.

Singh, P., X. Yu, A. Kumar, and A. K. Dubey. 2022. "Recent Advances in Silicate-Based Crystalline Bioceramics for Orthopedic Applications: A Review." *Journal of Materials Science* 57: 13109–13151. https://doi.org/10.1007/s10853-022-07444-w.

Smith, J. V. 1959. "The Crystal Structure of Proto-Enstatite, $MgSiO_3$." *Acta Crystallographica* 12: 515–519. https://doi.org/10.1107/S0365110X59001554.

Solórzano, L., and J. H. Sharp. 1980. "Determination of Total Dissolved Phosphorus and Particulate Phosphorus in Natural Waters." *Limnology and Oceanography* 25: 754–758. https://doi.org/10.4319/lo.1980.25.4.0754.

Souza, B., R. Souza, I. Santos, and E. Brocchi. 2020. "$MgSO_4$ Carbothermic Reductive Decomposition to Produce a Highly Reactive MgO Powder." *Journal of Materials Research and Technology* 9: 1847–1855. https://doi.org/10.1016/j.jmrt.2019.12.017.

Tovar-Sanchez, A., S. A. Sañudo-Wilhelmy, M. Garcia-Vargas, R. S. Weaver, L. C. Popels, and D. A. Hutchins. 2003. "A Trace Metal Clean Reagent to Remove Surface-Bound Iron from Marine Phytoplankton." *Marine Chemistry* 82: 91–99. https://doi.org/10.1016/s0304-4203(03)00054-9.

Supporting Information

Additional Supporting Information may be found in the online version of this article.

Submitted 24 September 2025
Revised 19 December 2025
Accepted 22 December 2025